Prevailing-frequency approximation of the coupling ray theory for S waves along the SH and SV reference rays in a transversely isotropic medium

Luděk Klimeš & Petr Bulant
Department of Geophysics, Faculty of Mathematics and Physics, Charles University in Prague, Ke Karlovu 3, 121 16 Praha 2, Czech Republic,
http://sw3d.cz/staff/klimes.htm, http://sw3d.cz/staff/bulant.htm

Summary

In an a priori known transversely isotropic medium, we can separate the slowness surface into the P–wave slowness sheet, the SH–wave slowness sheet and the SV–wave slowness sheet. We may then trace the SH rays and SV rays, and use them as the reference rays for the prevailing–frequency approximation of the coupling ray theory. In this way, we obtain two S–wave arrivals along each SH ray and have to select the correct one of them. Analogously, we obtain two S–wave arrivals along each SV ray and have to select the correct one of them. We propose how to select the correct arrivals in this paper. We then demonstrate the accuracy of the resulting prevailing–frequency approximation of the coupling ray theory for S waves along the SH and SV reference rays in two different transversely isotropic velocity models.

Keywords

Wave propagation, elastic anisotropy, transverse isotropy, heterogeneous media, S–wave coupling, prevailing frequency.

1. Introduction

In a generally anisotropic medium, the S–wave slowness sheets of the slowness surface are usually mostly separated and intersect in at up to 32 point S–wave singularities (Vavryčuk, 2005a; 2005b). In this case, outside the point singularities, the anisotropic–ray–theory rays stay at the faster or slower S–wave slowness sheet, respectively. When approaching the point singularities, the limiting case again corresponds to staying at the faster or slower S–wave slowness sheet, respectively. In a generally anisotropic medium, we thus have to separate the slowness surface into the P–wave slowness sheet, the faster S–wave slowness sheet and the slower S–wave slowness sheet.

However, in a transversely isotropic medium, the S–wave slowness sheets may intersect along intersection singularities (Vavryčuk, 2003). In this special case, we can separate the slowness surface into the P–wave slowness sheet, the SH–wave slowness sheet and the SV–wave slowness sheet.

Since any rounding error can perturb a transversely isotropic medium to a generally anisotropic medium and split the intersection singularity, we cannot determine numerically whether a medium is transversely isotropic. If a medium is transversely isotropic, we must know it a priori.

In an a priori known transversely isotropic medium, we can separate the SH and SV rays. To trace the SH rays, we need the SH eigenvector of the Christoffel matrix, the corresponding SH eigenvalue of the Christoffel matrix and its phase–space derivatives. For the coupling ray theory along the SH rays, we also need the SV eigenvector of the Christoffel matrix and the corresponding SV eigenvalue of the Christoffel matrix. Analogously for the SV rays.

The coupling ray theory Green tensor along the SH rays or along the SV rays can be calculated using the algorithm by Bulant & Klimeš (2002). The decomposition of the coupling ray theory Green tensor into two S–wave arrivals can be determined using the algorithm by Klimeš & Bulant (2012). In this way, we obtain two S–wave arrivals along each SH ray and have to select the correct one of them. Analogously, we obtain two S–wave arrivals along each SV ray and have to select the correct one of them. The Section 4 of this paper is devoted to the selection of the arrivals.

In Section 5, we demonstrate the accuracy of the resulting prevailing–frequency approximation of the coupling ray theory for S waves along the SH and SV reference rays in two different transversely isotropic velocity models QI2 and QI4. We compare the prevailing–frequency approximation along the SH and SV reference rays with the prevailing–frequency approximation along the anisotropic common S–wave rays and with the *Fourier pseudospectral method* (Pšenčík, Farra & Tessmer, 2012) which is considered as a nearly exact reference.

2. Perturbation approximation of travel time

We denote g_{k1} the SH eigenvector of the Christoffel matrix, and G_1 the corresponding SH eigenvalue of the Christoffel matrix. Then $G_1 = 1$ along the SH rays, but not along the SV rays. We analogously denote g_{k2} the SV eigenvector of the Christoffel matrix, and G_2 the corresponding SV eigenvalue of the Christoffel matrix. Then $G_2 = 1$ along the SV rays, but not along the SH rays.

During numerical calculation, the ray is divided into K sufficiently short segments indexed $k = 1, 2, ..., K$. The k^{th} ray segment extends from the $(k-1)^{\text{th}}$ point to the k^{th} point of the ray.

The increment $\Delta\tau_{1(k)}$ of SH travel time along the k^{th} segment of an SH ray is obtained by ray tracing. We may approximate the increment $\Delta\tau_{2(k)}$ of SV travel time along the k^{th} segment of an SH ray by linear perturbation expansion

$$\Delta\tau_{2(k)} = \tfrac{1}{2}\left[G_{1(k)}^{-\frac{1}{2}} + G_{1(k-1)}^{-\frac{1}{2}}\right]\Delta\tau_{1(k)} \quad , \tag{1}$$

where $G_{2(k-1)}$ and $G_{2(k)}$ are the SV eigenvalues of the Christoffel matrix at the initial point and endpoint of the ray segment, respectively.

Analogously, the increment $\Delta\tau_{2(k)}$ of SV travel time along the k^{th} segment of an SV ray is obtained by ray tracing, and we may approximate the increment $\Delta\tau_{1(k)}$ of SH travel time along the k^{th} segment of an SV ray by linear perturbation expansion

$$\Delta\tau_{1(k)} = \tfrac{1}{2}\left[G_{1(k)}^{-\frac{1}{2}} + G_{1(k-1)}^{-\frac{1}{2}}\right]\Delta\tau_{2(k)} \quad , \tag{2}$$

where $G_{1(k-1)}$ and $G_{1(k)}$ are the SH eigenvalues of the Christoffel matrix at the initial point and endpoint of the ray segment, respectively.

We may also improve the accuracy of linear perturbation expansions (1) and (2) by including the second–order perturbations of travel time according to Klimeš (2002), Klimeš & Bulant (2006) and Bulant & Klimeš (2008).

3. Prevailing–frequency approximation of the coupling ray theory

The algorithm of calculating the prevailing–frequency approximation of the coupling ray theory S–wave Green tensor is equal along the SH rays and SV rays.

At the k^{th} point of the ray, we need to know the SH eigenvector $g_{i1(k)}$ of the Christoffel matrix and the SV eigenvector $g_{i2(k)}$ of the Christoffel matrix.

Along the k^{th} ray segment, we determine the rotation

$$\Delta\varphi_{(k)} = \arctan\left(\frac{g_{i1(k)}g_{i2(k-1)} - g_{i2(k)}g_{i1(k-1)}}{g_{j1(k)}g_{j1(k-1)} + g_{j2(k)}g_{j2(k-1)}} \right) \tag{3}$$

(Bulant & Klimeš, 2002, eq. 18) of the S–wave eigenvectors of the Christoffel matrix, the increment

$$\Delta\overline{\tau}_{(k)} = \tfrac{1}{2}\left(\Delta\tau_{1(k)} + \Delta\tau_{2(k)}\right) \tag{4}$$

(Bulant & Klimeš, 2002, eq. 20; Klimeš & Bulant, 2012, eq. 6) of mean travel time $\overline{\tau}$, and quantity

$$\Delta\varepsilon_{(k)} = \tfrac{1}{2}\,\omega_0\left(\Delta\tau_{2(k)} - \Delta\tau_{1(k)}\right) \tag{5}$$

(Bulant & Klimeš, 2002, eq. 21; Klimeš & Bulant, 2012, eq. 2), where ω_0 is the prevailing circular frequency.

We calculate the propagator matrix $\mathbf{\Pi}$ of the coupling equations and its frequency derivative $\mathbf{D}$ using the algorithm by Klimeš & Bulant (2012, sec. 4). Along the k^{th} ray segment, we determine

$$\alpha_{(k)} = \sqrt{(\Delta\varphi_{(k)})^2 + (\Delta\varepsilon_{(k)})^2} \tag{6}$$

(Bulant & Klimeš, 2002, eq. 15; Klimeš & Bulant, 2012, eq. 51) and 2×2 complex–valued matrix

$$\mathbf{A}_{(k)} = \begin{pmatrix} 0 & 1 \\ -1 & 0 \end{pmatrix} \frac{\Delta\varphi_{(k)}}{\alpha_{(k)}} - \begin{pmatrix} \mathrm{i} & 0 \\ 0 & -\mathrm{i} \end{pmatrix} \frac{\Delta\varepsilon_{(k)}}{\alpha_{(k)}} \tag{7}$$

Bulant & Klimeš, 2002, eq. 14; Klimeš & Bulant, 2012, eq. 50). The propagator matrix of the coupling equations along the k^{th} ray segment reads

$$\Delta\mathbf{\Pi}_{(k)} = \mathbf{1}\cos(\alpha_{(k)}) + \mathbf{A}_{(k)}\sin(\alpha_{(k)}) \tag{8}$$

(Červený, 2001, eq. 5.4.86; Bulant & Klimeš, 2002, eq. 17; Klimeš & Bulant, 2012, eq. 49). The derivative of $\Delta\mathbf{\Pi}_{(k)}$ with respect to prevailing circular frequency ω_0 is

$$\Delta\mathbf{D}_{(k)} = \left\{ \left[-\mathbf{1}\sin(\alpha_{(k)}) + \mathbf{A}_{(k)}\cos(\alpha_{(k)}) - \mathbf{A}_{(k)}\frac{\sin(\alpha_{(k)})}{\alpha_{(k)}} \right] \frac{\Delta\varepsilon_{(k)}}{\alpha_{(k)}} - \begin{pmatrix} \mathrm{i} & 0 \\ 0 & -\mathrm{i} \end{pmatrix} \frac{\sin(\alpha_{(k)})}{\alpha_{(k)}} \right\} \frac{\Delta\varepsilon_{(k)}}{\omega} \tag{9}$$

(Klimeš & Bulant, 2012, eq. 56).

At the initial point of the ray, we set

$$\mathbf{\Pi}_{(0)} = \mathbf{1} \tag{10}$$

(Klimeš & Bulant, 2012, eq. 46). and

$$\mathbf{D}_{(0)} = \mathbf{0} \tag{11}$$

(Klimeš & Bulant, 2012, eq. 52). At the subsequent points of the ray, we calculate

$$\mathbf{\Pi}_{(k)} = \Delta\mathbf{\Pi}_{(k)}\mathbf{\Pi}_{(k-1)} \quad , \qquad k = 1, 2, ..., K \tag{12}$$

(Klimeš & Bulant, 2012, eq. 47) and

$$\mathbf{D}_{(k)} = \Delta\mathbf{\Pi}_{(k)}\mathbf{D}_{(k-1)} + \Delta\mathbf{D}_{(k)}\mathbf{\Pi}_{(k-1)} \quad , \qquad k = 1, 2, ..., K \tag{13}$$

(Klimeš & Bulant, 2012, eq. 53). The resulting propagator matrix $\mathbf{\Pi}$ and its frequency derivative $\mathbf{D}$ are

$$\mathbf{\Pi} = \mathbf{\Pi}_{(K)} \tag{14}$$

(Klimeš & Bulant, 2012, eq. 48) and

$$\mathbf{D} = \mathbf{D}_{(K)} \tag{15}$$

(Klimeš & Bulant, 2012, eq. 54).

We calculate difference D of the coupling–ray–theory travel times from mean travel time

$$\overline{\tau} = \sum_{k=0}^{K} \Delta\overline{\tau}_{(k)} \tag{16}$$

using relation

$$D = \sqrt{\det[\mathbf{D}(\omega_0)]} \tag{17}$$

(Klimeš & Bulant, 2012, eq. 21). We then calculate 2×2 complex–valued singular amplitude matrices

$$\mathbf{\Pi}^{(1)} = \frac{1}{2}\left[\mathbf{\Pi} + \mathrm{i}\frac{\mathbf{D}}{D}\right] \tag{18}$$

(Klimeš & Bulant, 2012, eq. 22), and

$$\mathbf{\Pi}^{(2)} = \frac{1}{2}\left[\mathbf{\Pi} - \mathrm{i}\frac{\mathbf{D}}{D}\right] \quad . \tag{19}$$

(Klimeš & Bulant, 2012, eq. 23).

4. Selection of arrivals

For each SH ray, we now have two arrivals with coupling–ray–theory travel times $\overline{\tau} - D$ and $\overline{\tau} + D$, and singular amplitude matrices $\mathbf{\Pi}^{(1)}$ and $\mathbf{\Pi}^{(2)}$, respectively. We need to select just one of them. We may try to select the proper arrival according to its polarization or travel time. If one of the arrivals is close to the anisotropic–ray–theory SH arrival by its polarization and its travel time, we may assume that it is probably calculated with a good accuracy and select it. If this selection fails, the coupling ray theory along SH and SV reference rays can not be used, and we should calculate the coupling–ray–theory approximation along the anisotropic common S–wave rays. Analogously for each SV ray.

4.1. Selection of arrivals based on polarization

We obtain the anisotropic–ray–theory approximation by setting

$$\mathbf{\Pi}^{\mathrm{SH}} = \begin{pmatrix} 1 & 0 \\ 0 & 0 \end{pmatrix} \tag{20}$$

and

$$\mathbf{\Pi}^{\mathrm{SV}} = \begin{pmatrix} 0 & 0 \\ 0 & 1 \end{pmatrix} \quad . \tag{21}$$

Along the SH ray, we may thus select the arrival according to component $\Pi_{11}^{(1)}$ of matrix $\mathbf{\Pi}^{(1)}$ and component $\Pi_{11}^{(2)}$ of matrix $\mathbf{\Pi}^{(2)}$:

$$|\Pi_{11}^{(1)}| \gg |\Pi_{11}^{(2)}| \quad \Longrightarrow \quad \tau^{\mathrm{SH}} = \overline{\tau} - D \quad , \quad \mathbf{\Pi}^{\mathrm{SH}} = \mathbf{\Pi}^{(1)} \tag{22}$$

or

$$|\Pi_{11}^{(2)}| \gg |\Pi_{11}^{(1)}| \quad \Longrightarrow \quad \tau^{\mathrm{SH}} = \overline{\tau} + D \quad , \quad \mathbf{\Pi}^{\mathrm{SH}} = \mathbf{\Pi}^{(2)} \quad . \tag{23}$$

Along the SV ray, we may thus select the arrival analogously according to component $\Pi_{22}^{(1)}$ of matrix $\mathbf{\Pi}^{(1)}$ and component $\Pi_{22}^{(2)}$ of matrix $\mathbf{\Pi}^{(2)}$:

$$|\Pi_{22}^{(1)}| \gg |\Pi_{22}^{(2)}| \quad \Longrightarrow \quad \tau^{\mathrm{SV}} = \overline{\tau} - D \quad , \quad \mathbf{\Pi}^{\mathrm{SV}} = \mathbf{\Pi}^{(1)} \tag{24}$$

or

$$|\Pi_{22}^{(2)}| \gg |\Pi_{22}^{(1)}| \quad \Longrightarrow \quad \tau^{\mathrm{SV}} = \overline{\tau} + D \quad , \quad \mathbf{\Pi}^{\mathrm{SV}} = \mathbf{\Pi}^{(2)} \quad . \tag{25}$$

If both conditions (22) and (23) fail, or both conditions (24) and (25) fail, this selection of arrivals based on polarization fails.

4.2. Selection of arrivals based on travel time

The selection of arrivals along the SH ray according to the SH anisotropic–ray–theory travel time τ_1 is possible only if both $|\tau_1 - \overline{\tau}|$ and D are not negligible with respect to τ_1. Then

$$\tau_1 - \overline{\tau} < 0 \quad \Longrightarrow \quad \tau^{\mathrm{SH}} = \overline{\tau} - D \quad , \quad \mathbf{\Pi}^{\mathrm{SH}} = \mathbf{\Pi}^{(1)} \tag{26}$$

or

$$\tau_1 - \overline{\tau} > 0 \quad \Longrightarrow \quad \tau^{\mathrm{SH}} = \overline{\tau} + D \quad , \quad \mathbf{\Pi}^{\mathrm{SH}} = \mathbf{\Pi}^{(2)} \quad . \tag{27}$$

Analogously, the selection of arrivals along the SV ray according to the SV anisotropic–ray–theory travel time τ_2 is possible only if both $|\tau_2 - \overline{\tau}|$ and D are not negligible with respect to τ_2. Then

$$\tau_2 - \overline{\tau} < 0 \quad \Longrightarrow \quad \tau^{\mathrm{SV}} = \overline{\tau} - D \quad , \quad \mathbf{\Pi}^{\mathrm{SV}} = \mathbf{\Pi}^{(1)} \tag{28}$$

or

$$\tau_2 - \overline{\tau} > 0 \quad \Longrightarrow \quad \tau^{\mathrm{SV}} = \overline{\tau} + D \quad , \quad \mathbf{\Pi}^{\mathrm{SV}} = \mathbf{\Pi}^{(2)} \quad . \tag{29}$$

This selection of arrivals based on travel time is recommended especially as the test of the selection of arrivals based on polarization.

4.3. Complex–valued Green–tensor amplitude

If the selection of arrivals is successful, the coupling–ray–theory SH Green tensor has travel time τ^{SH} and complex–valued tensorial amplitude

$$A_{ij}^{\mathrm{SH}} = A^{\mathrm{SH}}\, g_{iI(K)}^{\mathrm{SH}}\, \Pi_{IJ}^{\mathrm{SH}}\, g_{jJ(0)}^{\mathrm{SH}}\, \exp\bigl[\mathrm{i}\omega_0\bigl(\overline{\tau} - \tau^{\mathrm{SH}}\bigr)\bigr] \quad , \tag{30}$$

and the coupling–ray–theory SV Green tensor has travel time τ^{SV} and complex–valued tensorial amplitude

$$A_{ij}^{\mathrm{SV}} = A^{\mathrm{SV}}\, g_{iI(K)}^{\mathrm{SV}}\, \Pi_{IJ}^{\mathrm{SV}}\, g_{jJ(0)}^{\mathrm{SV}}\, \exp\bigl[\mathrm{i}\omega_0\bigl(\overline{\tau} - \tau^{\mathrm{SV}}\bigr)\bigr] \quad , \tag{31}$$

see Klimeš & Bulant (2012, eqs. 43–44). Here ω_0 is the prevailing circular frequency, A^{SH} is the complex–valued scalar amplitude of the Green tensor (Klimeš, 2014) corresponding to the anisotropic–ray–theory SH wave, A^{SV} is the complex–valued scalar amplitude of the Green tensor (Klimeš, 2014) corresponding to the anisotropic–ray–theory SV wave, g_{i1}^{SH} is the SH eigenvector of the Christoffel matrix calculated along the SH ray, g_{i2}^{SH} is the SV eigenvector of the Christoffel matrix calculated along the SH ray, g_{i1}^{SV} is the SH eigenvector of the Christoffel matrix calculated along the SV ray, and g_{i2}^{SV} is the SV eigenvector of the Christoffel matrix calculated along the SV ray.

5. Numerical examples

Bulant et al. (2011) and Klimeš & Bulant (2012) compared the coupling ray theory for S waves and its prevailing–frequency approximation with the *Fourier pseudospectral method* (Pšenčík, Farra & Tessmer, 2012) which was considered as a nearly exact reference. Four velocity models QI, QI2, QI4 and KISS of seven velocity models used for the comparison with nearly exact reference seismograms are transversely isotropic. These transversely isotropic velocity models display no intersection singularity. The anisotropy of velocity models QI and KISS is weak enough for the anisotropic–common–ray approximation of the coupling ray theory to yield almost exact seismograms (Klimeš & Bulant, 2012, Figs. 3, 8). We thus compare the prevailing–frequency approximation of the coupling ray theory with the Fourier pseudospectral method in velocity models QI2 and QI4. We consider the prevailing–frequency approximation of the coupling ray theory calculated (a) along the anisotropic common S–wave reference rays with the quadratic perturbation expansions of travel times (b) along the SH and SV reference rays with the linear perturbation expansions (1) and (2) of travel times.

5.1. Anisotropic velocity models

We thus consider two weakly anisotropic velocity models referred to as QI2 and QI4. Both these velocity models are laterally homogeneous. The density is constant. The elastic moduli are linear functions of depth.

A vertically heterogeneous 1–D anisotropic velocity models QI2 and QI4 are transversely isotropic in a vertical plane which forms a 45° angle with the source–receiver vertical plane and is situated between the positive radial and positive transverse seismogram components. Velocity models QI2 and QI4 are derived from velocity model QI (Pšenčík & Dellinger, 2001, model WA rotated by 45°) and mutually differ by their degrees of anisotropy. The differences of the elastic moduli in velocity models QI, QI2 and QI4 from the elastic moduli in the reference isotropic velocity model are determined by ratio $1:2:4$. For the elastic moduli in velocity models QI2 and QI4 refer to Bulant & Klimeš (2008).

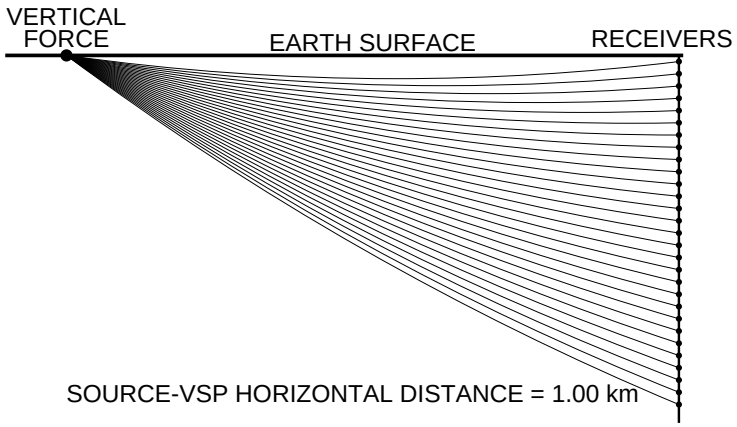

Figure 1: The source–receiver configuration for the calculation of synthetic seismograms, with a sketch of the reference rays. The source is located at the Earth's surface, the receivers are placed in the vertical well.

5.2. Measurement configuration

The synthetic seismograms generated by a vertical force are calculated at the receivers located in a vertical well at a distance of 1 km from the source. The source–receiver configuration in velocity models QI2 and QI4 is displayed in Figure 1.

The source time function is the Gabor signal $\cos(2\pi ft)\exp[-(2\pi ft/4)^2]$ with reference frequency $f = 50\,\mathrm{Hz}$, bandpass filtered by a cosine filter specified by frequencies 0 Hz, 5 Hz, 60 Hz and 100 Hz. The depths of the receivers are displayed in the plots of seismograms. The receivers record the following 3 components of displacement: radial component (along the line connecting the source and the top of the well, positive away from the source), transverse component (perpendicular to the source–receiver plane), and vertical component (positive downwards). The recording system is right–handed. For the prevailing–frequency approximation of the coupling ray theory, we naturally use prevailing frequency $f_0 = 50\,\mathrm{Hz}$.

5.3. Comparison of synthetic seismograms

The synthetic seismograms in velocity models QI2 and QI4 are displayed in Figures 2–5. In both velocity models, we compare the prevailing–frequency approximation of the coupling ray theory along the anisotropic common S–wave reference rays with the Fourier pseudospectral method, and the prevailing–frequency approximation of the coupling ray theory along the SH and SV reference rays with the Fourier pseudospectral method. In each figure, the synthetic seismograms calculated by the prevailing–frequency approximation of the coupling ray theory and by the Fourier pseudospectral method are displayed in different colours. In each velocity model, the amplitude scaling is equal for all components and all receivers. Note that the second (transverse) component would vanish in the isotropic–ray–theory seismograms in these velocity models.

Along the anisotropic common S–wave reference rays, we use the quadratic perturbation expansions of travel times because they yield slightly more accurate synthetic seismograms than linear expansions. Along the SH and SV reference rays, we use the linear perturbation expansions (1) and (2) of travel times, and the presented numerical examples suggest that the linear perturbation expansions are sufficiently accurate in velocity models QI2 and QI4. Since transversely isotropic velocity models QI2 and QI4 display no intersection singularity, we applied the selection of arrivals based on travel

time according to Section 4.2 in these velocity models. In these early numerical tests, we selected the arrivals manually.

In velocity model QI2 (Figures 2 and 3) which displays the development of S–wave splitting, we can observe that the amplitude differences in the third (vertical) component and also in the first (radial) component (first S–wave arrival at the bottom receivers) have been corrected by the prevailing–frequency approximation of the coupling ray theory along the SH and SV reference rays.

Velocity model QI4 (Figures 4 and 5), whose anisotropy is twice stronger than in model QI2, is considerably anisotropic, and the separation of the two S waves is about 0.06 s which corresponds approximately to three S–wave periods. In velocity model QI4, the amplitude differences in the third (vertical) component, and also in the second (transverse) component (first S–wave arrival at deeper receivers) and in the first (radial) component (first S–wave arrival at deeper receivers) have been corrected by the prevailing–frequency approximation of the coupling ray theory along the SH and SV reference rays.

6. Discussion

When we apply the prevailing–frequency approximation of the coupling ray theory to the SH and SV reference rays in a transversely isotropic medium, we do not know a priori whether the proposed selection of arrivals is possible and successful.

If the proposed selection of arrivals is successful, we may expect that one of the two coupling–ray–theory arrivals obtained along each ray is very accurate while the other is less accurate than for a common S–wave reference ray. *It has to be theoretically derived whether the combination of the selected accurate arrivals forms a Green tensor within the high–frequency limit.*

The numerical tests performed in transversely isotropic velocity models QI2 and QI4 showed that the selection of arrivals was possible and that the prevailing–frequency approximation of the coupling ray theory along the SH and SV reference rays provided correct seismograms in these two velocity models. However, these velocity models display no intersection singularity.

The proposed prevailing–frequency approximation of the coupling ray theory along the SH and SV reference rays has to be compared further with the exact solution and with the coupling ray theory along the common S–wave reference rays, especially in the vicinities of the kiss and intersection singularities.

Acknowledgements

We are grateful to Einar Iversen who encouraged us in this study. Ekkehart Tessmer kindly applied his Fourier pseudospectral method to calculating the seismograms which we used here as nearly exact reference seismograms.

The research has been supported by the Grant Agency of the Czech Republic under contract P210/10/0736, by the Ministry of Education of the Czech Republic within research projects MSM0021620860 and CzechGeo/EPOS LM2010008, and by the members of the consortium "Seismic Waves in Complex 3–D Structures" (see "http://sw3d.cz").

References

Bulant, P. & Klimeš, L. (2002): Numerical algorithm of the coupling ray theory in weakly anisotropic media. *Pure appl. Geophys.*, **159**, 1419–1435.

Bulant, P. & Klimeš, L. (2008): Numerical comparison of the isotropic–common–ray and anisotropic–common–ray approximations of the coupling ray theory. *Geophys. J. int.*, **175**, 357–374.

Bulant, P., Pšenčík, I., Farra, V. & Tessmer, E. (2011): Comparison of the anisotropic-common-ray approximation of the coupling ray theory for S waves with the Fourier pseudo-spectral method in weakly anisotropic models. In: *Seismic Waves in Complex 3–D Structures, Report 21*, pp. 167–183, Dep. Geophys., Charles Univ., Prague, online at "http://sw3d.cz".

Červený, V. (2001): *Seismic Ray Theory.* Cambridge Univ. Press, Cambridge.

Klimeš, L. (2002): Second–order and higher–order perturbations of travel time in isotropic and anisotropic media. *Stud. geophys. geod.*, **46**, 213–248.

Klimeš, L. (2014): Calculation of the amplitudes of elastic waves in anisotropic media in Cartesian or ray–centred coordinates. *Seismic Waves in Complex 3–D Structures*, **24**, 111–126, online at "http://sw3d.cz".

Klimeš, L. & Bulant, P. (2006): Errors due to the anisotropic–common–ray approximation of the coupling ray theory. *Stud. geophys. geod.*, **50**, 463–477.

Klimeš, L. & Bulant, P. (2012): Single–frequency approximation of the coupling ray theory. In: *Seismic Waves in Complex 3–D Structures, Report 22*, pp. 143–167, Dep. Geophys., Charles Univ., Prague, online at "http://sw3d.cz".

Pšenčík, I. & Dellinger, J. (2001): Quasi–shear waves in inhomogeneous weakly anisotropic media by the quasi–isotropic approach: A model study. *Geophysics*, **66**, 308–319.

Pšenčík, I., Farra, V. & Tessmer, E. (2012): Comparison of the FORT approximation of the coupling ray theory with the Fourier pseudospectral method. *Stud. geophys. geod.*, **56**, 35–64.

Vavryčuk, V. (2003): Generation of triplications in transversely isotropic media. *Phys. Rev. B*, **68**, 054107-1–054107-8.

Vavryčuk, V. (2005a): Acoustic axes in weak triclinic anisotropy. *Geophys. J. int.*, **163**, 629–638.

Vavryčuk, V. (2005b): Acoustic axes in triclinic anisotropy. *J. acoust. Soc. Am.*, **118**, 647–653.

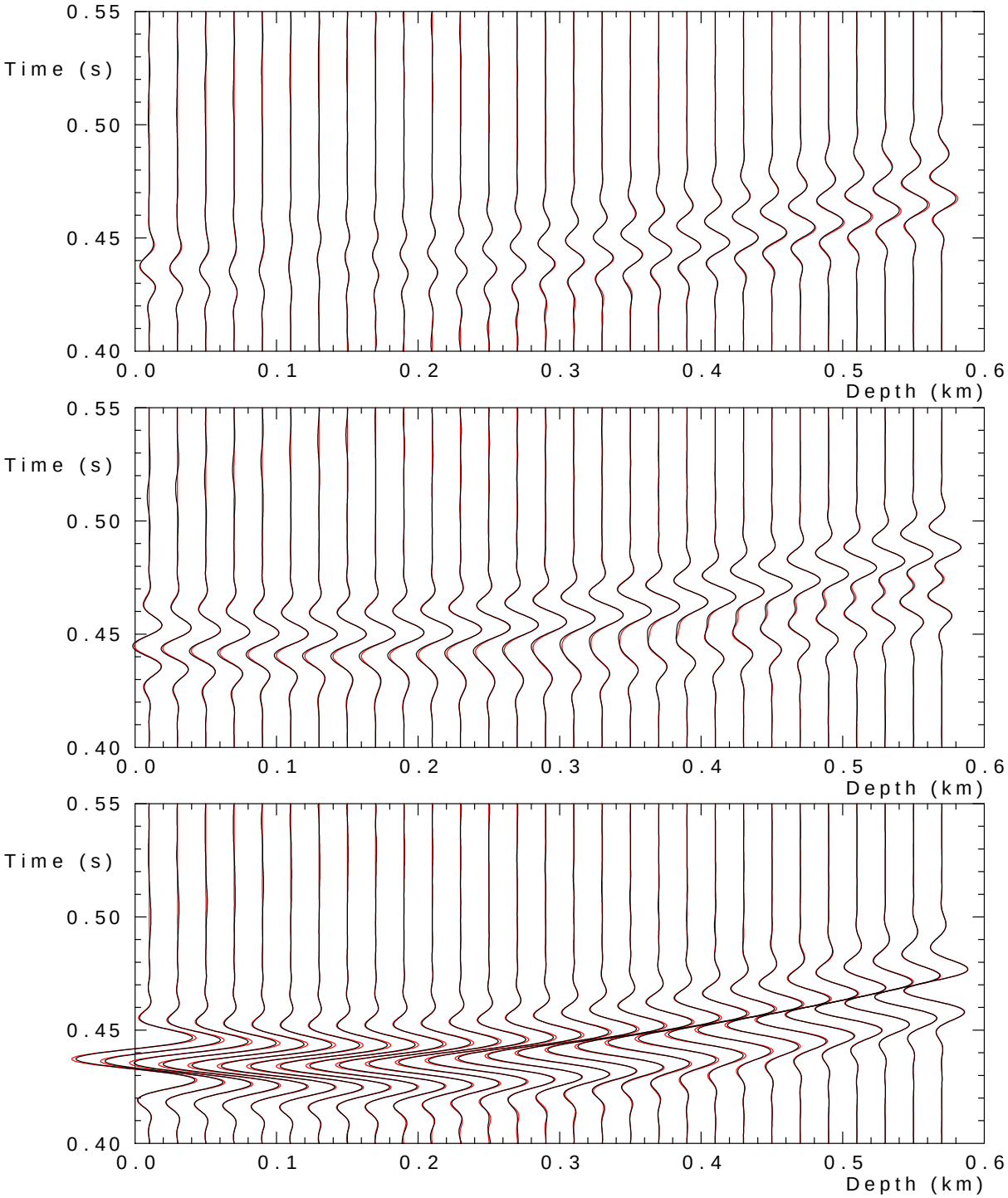

Figure 2: Radial, transverse and vertical component of the seismograms calculated in velocity model QI2. The **red** seismograms are calculated using the prevailing–frequency approximation of the coupling ray theory according to Klimeš & Bulant (2012) along the anisotropic common S–wave rays with the quadratic perturbation expansions of travel times. They are overlaid by the **black** seismograms calculated using the Fourier pseudospectral method by Pšenčík, Farra & Tessmer (2012) which is considered here as a nearly exact reference.

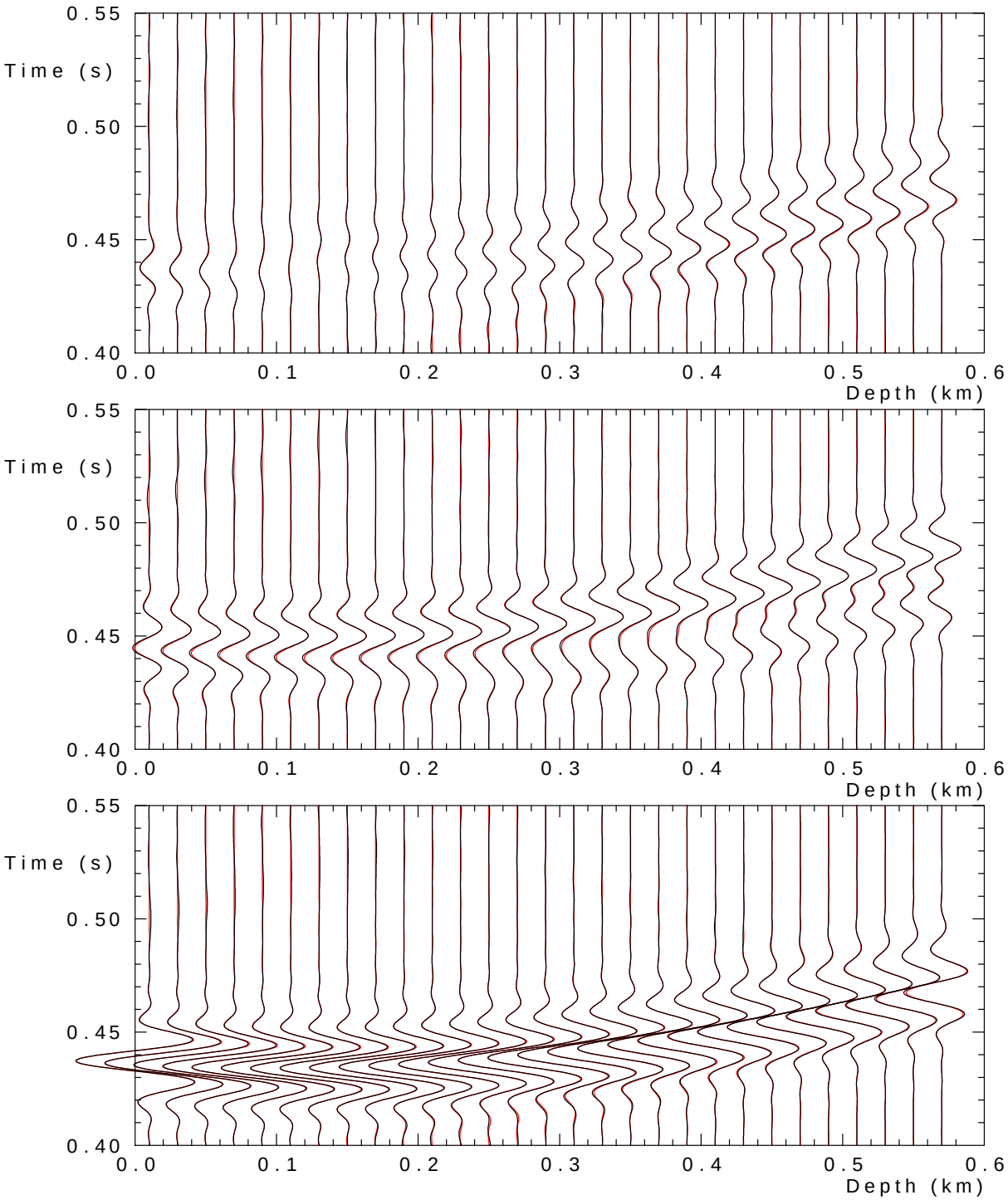

Figure 3: Radial, transverse and vertical component of the seismograms calculated in velocity model QI2. The **red** seismograms are calculated using the prevailing–frequency approximation of the coupling ray theory according to Klimeš & Bulant (2012) along the SH and SV reference rays with the linear perturbation expansions of travel times as described in this paper. They are overlaid by the **black** seismograms calculated using the Fourier pseudospectral method by Pšenčík, Farra & Tessmer (2012) which is considered here as a nearly exact reference. In comparison with Figure 2, the amplitude differences in the third (vertical) component and also in the first (radial) component (first S–wave arrival at the bottom receivers) have been corrected.

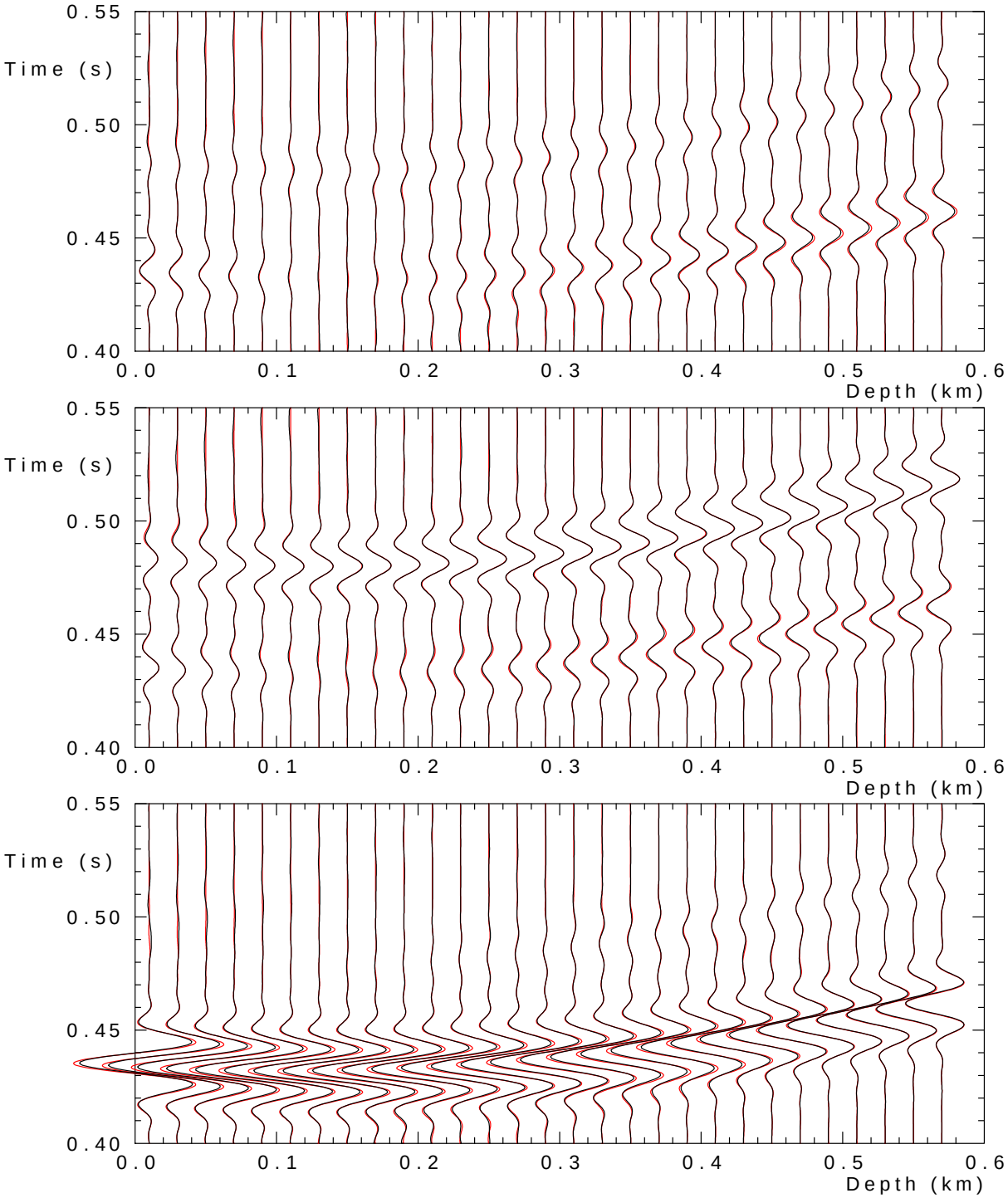

Figure 4: Radial, transverse and vertical component of the seismograms calculated in velocity model QI4. The **red** seismograms are calculated using the prevailing–frequency approximation of the coupling ray theory according to Klimeš & Bulant (2012) along the anisotropic common S–wave rays with the quadratic perturbation expansions of travel times. They are overlaid by the **black** seismograms calculated using the Fourier pseudospectral method by Pšenčík, Farra & Tessmer (2012) which is considered here as a nearly exact reference.

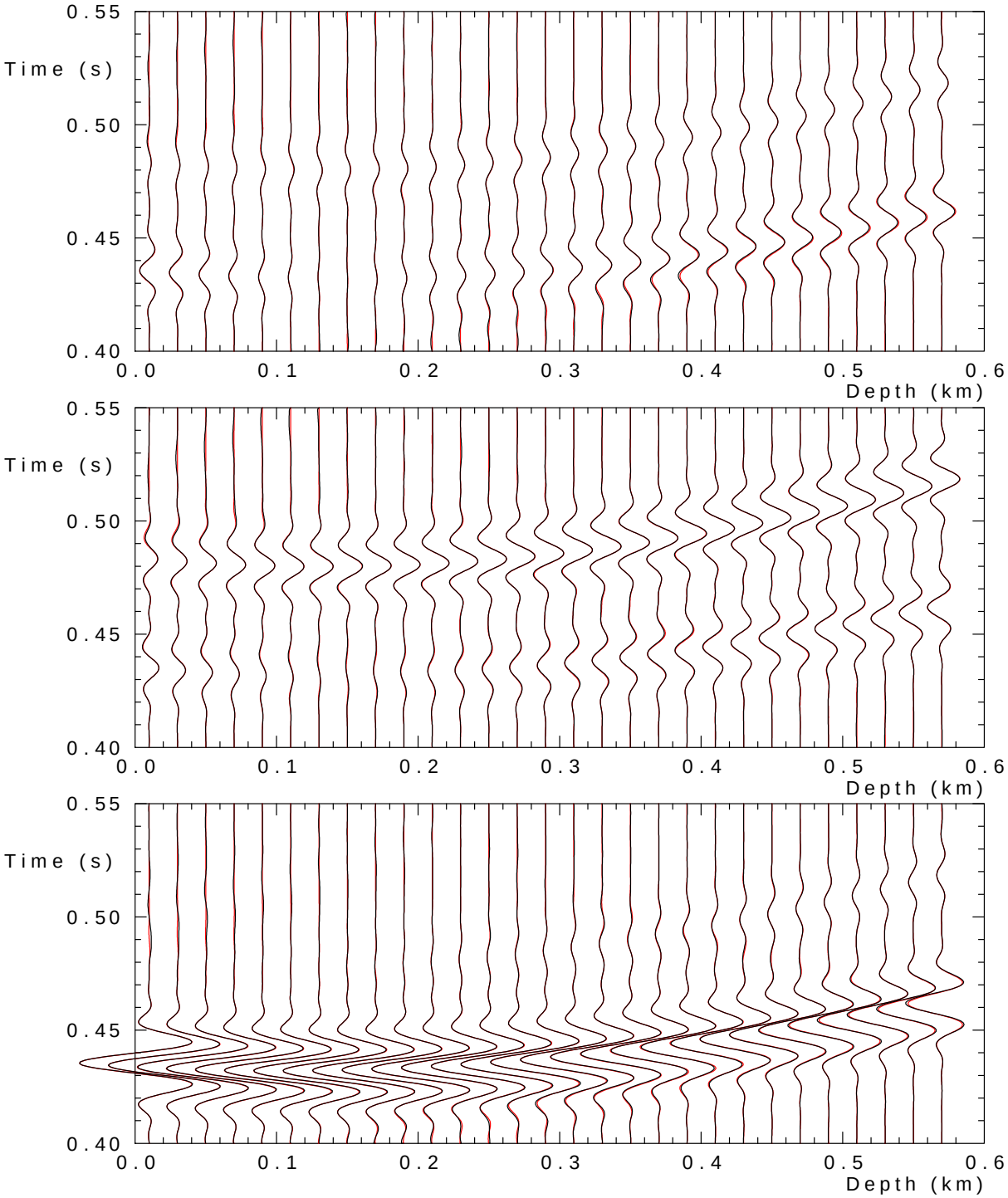

Figure 5: Radial, transverse and vertical component of the seismograms calculated in velocity model QI4. The **red** seismograms are calculated using the prevailing–frequency approximation of the coupling ray theory according to Klimeš & Bulant (2012) along the SH and SV reference rays with the linear perturbation expansions of travel times as described in this paper. They are overlaid by the **black** seismograms calculated using the Fourier pseudospectral method by Pšenčík, Farra & Tessmer (2012) which is considered here as a nearly exact reference. In comparison with Figure 4, the amplitude differences in the third (vertical) component, and also in the second (transverse) component (first S–wave arrival at deeper receivers) and in the first (radial) component (first S–wave arrival at deeper receivers) have been corrected.